CO_2 methanation: deciphering the role of dopants (Mn, Co, and Cu) in Ni/SiO_2 catalysts prepared by sol-gel chemistry

Yingrui Zhao,[a] Sandra Casale, [b] Capucine Sassoye,[c] Damien P. Debecker [a,*]

[a] Université catholique de Louvain (UCLouvain), Institute of Condensed Matter and Nanosciences (IMCN), Place Louis Pasteur, 1, box L4.01.09, 1348 Louvain-La-Neuve, Belgium.
[b] Sorbonne Université, Laboratoire de Réactivité de Surface, CNRS UMR 7197, 4 Place Jussieu, 75005, Paris, France
[c] Sorbonne Université, Chimie de la Matière Condensée de Paris, UMR 7574, 4 Place Jussieu, 75005 Paris, France.

* Corresponding autor:
E-mail: damien.debecker@uclouvain.be
ORCID: 0000-0001-6500-2996

Abstract

CO_2 methanation is effectively catalyzed by Ni-based catalysts, and reactivity can be further tuned by the addition of promoters. Deciphering the relationship between the promoter in Ni-based catalysts and the corresponding catalytic performance in CO_2 methanation mechanism is of great meaning for the development of highly active catalysts. Herein, a series of model bimetallic catalysts were prepared by sol-gel chemistry to address this fundamental challenge. Compared to Ni/SiO_2 catalyst, the Mn-doped and Co-doped catalysts showed a higher methanation activity, with the former showing better performance below 250 °C and the latter showing better performance over 300 °C. On the contrary, the Cu-promoted catalyst showed a lower CO_2 conversion with a lower CH_4 selectivity in the whole temperature range. A comprehensive characterization study (TEM, XRD, XPS, H_2-TPR, CO_2-TPD, in situ DRIFTS, and TPSR analyses) suggests that the effect of promoters is not directly related to improvement of dispersion, reducibility, or basicity. Instead, we show that the promoters orient the reaction mechanism and favor the conversion of key intermediates. Mn addition has the highest promoting effect on the hydrogenation of formaldehyde intermediate ($*OCH_2$) to methoxy intermediate ($*OCH_3$), i.e. the rate determining step of the "RWGS+CO hydrogenation" pathway which is shown to predominate at low reaction temperature. Co addition facilitates the formation of formate species, i.e. the rate determining step of the formate pathway which is also active at high reaction temperature. Cu addition has a negative effect on the rate determining step of those two pathways, resulting a lower performance of $Ni-Cu/SiO_2$.

Keywords

Hydrogenation of CO_2, Sabatier reaction, metal doping, Ni nanoparticles, mesoporous catalysts

1. Introduction

Anthropogenic CO_2 emissions, provoked by the massive combustion of fossil fuels, are the cause of major climatic and environmental issues we are facing today. CO_2 capture and storage (CCS) and CO_2 capture and utilization (CCU) have been extensively studied and proposed as relevant mitigation technologies.[1-3] Generally, CO_2 can be catalytically converted into fuels or commodity chemicals (such as carbon monoxide, methane, methanol, formic acid, ethanol, etc.).[4-9] Among them, CH_4 is a promising target as it is in great demand and amenable to cost-effective utilization via existing distribution and combustion systems.[10] Importantly, the hydrogen used for the CO_2 methanation must be "green", i.e. supplied from the water electrolysis (fed with renewable electricity) or photocatalysis, which provides a way to store the surplus of intermittent renewable energy.[11, 12]

As a highly exothermic reaction, CO_2 methanation reaction ($CO_2 + 4H_2 \rightarrow CH_4 + 2H_2O$, ΔH_{298K} = -165 kJ mol^{-1}) is favored at low temperature. Furthermore, at high temperature, CO can be produced as a byproduct and catalyst deactivation process is accelerated.[6] On the contrary, this process is kinetically limited due to the high stability of CO_2 and the substantial energy demand to transform C^{4+} of CO_2 to C^{4-} of CH_4.[13] Therefore, the major goal in this filed is developing high activity catalysts that allow operating the reaction at a relatively low temperature, while maintaining high CH_4 selectivity and stability.

Supported Ni-based catalysts are the most promising candidate for the CO_2 methanation reaction due to their high CH_4 selectivity and low cost.[14] However, the activity of Ni-based catalysts at low temperature is lower than that of some noble metal counterparts. To improve catalytic activity, various promoters have been investigated. Reports from the literature are somewhat controversial, showing that promoters can have various effects: alter the dispersion of the active component (Ni nanoparticles), modify the ability to be reduced during pretreatment, enhance the surface basicity, and possibly modify the reaction pathways.[15-18] Wu et al. reported that Mn-doped Ni/Al_2O_3-ZrO_2 catalysts exhibited the best catalytic activity in comparison to other additives (Fe, Co, Cr).[19] On the contrary, Xu et al. found that the Co-doped catalysts

exhibited much higher activity than the Mn-, Fe-, and Cu-doped catalysts in the $Ni/Ce_{0.8}Zr_{0.2}O_2$ system.[20] These contrasting observations may result from the use of different "non-innocent" supports. To decipher the actual effect of the metal dopant on Ni-based methanation catalyst, it appears relevant to focus on an inert support.

Herein, a series of Ni-M/SiO_2 (M = Mn, Co, Cu) bimetallic catalysts was prepared by adapting an ethylene glycol-assisted sol-gel method that was recently shown to lead to finely dispersed Ni metal nanoparticles embedded in a mesoporous silica matrix.[21] Doping with Cu was found counter-productive, with a marked activity drop for Ni-Cu/SiO_2 compared to pristine Ni/SiO_2. On the contrary, we found that Mn and Co addition improved the CO_2 methanation activity of the Ni/SiO_2 catalyst. On the one hand, the Mn-doped catalyst shows high activity at relatively low temperature (below 250 °C). Co addition, on the other hand, particularly improved the CO_2 methanation activity at relatively high temperature (over 300 °C). Using a combination of characterization techniques, we elucidate the doping effect on (i) the catalyst properties and (ii) on the CO_2 methanation mechanism.

2. Experimental section

2.1. Catalyst preparation.

The bimetallic Ni-M/SiO_2 (M = Mn, Co, and Cu) and a monometallic Ni/SiO_2 were both prepared by a sol-gel method (Scheme 1). Typically, anhydrous ethanol (EtOH), distilled H_2O, and HNO_3 were added to tetraethyl orthosilicate (TEOS) at a molar ratio of 3:1.8:0.03:1 and stirred for 1 h to obtain a clear SiO_2 sol. The required amount of $Ni(NO_3)_2 \cdot 6H_2O$ and transition metals (Mn, Co, and Cu) nitrates were dissolved in into ethylene glycol (EG) and methanol (V_{EG}:$V_{methanol}$ = 3:2), and the solution was maintained at 2 M of metal salts (Ni + dopant). The solution was then added to the SiO_2 sol and stirred for another 1 h. The obtained slurry was aged at 30 °C for 12 h and dried at 120 °C for another 12 h to form a gel. The dried gel was calcined in air at 300 °C (1 °C/min) for 2 h, and then at 500 °C (1 °C/min) for an additional 2 h. The mass fraction of nickel loading was fixed at 20% for all the catalysts and the theoretical mass ratio for Ni/M (M = Mn, Co, and Cu) was fixed at 4. The calcined sample were denoted

as “Ni-M/SiO_2”. The calcined catalyst was reduced in situ in the reactor under a H_2/He flow (see below), and the corresponding samples were denoted “Ni-M/SiO_2-r”.

2.2. Characterization.

N_2 adsorption-desorption analyses were carried out on a Tristar 3000 (Micromeritics, USA) instrument. The sample was degassed at 250 °C for 3 h to remove physically adsorbed water and impurities on the surface before the measurement. The total pore volume (V_p) was calculated from the amount of nitrogen absorbed at a P/P_0 of 0.98 and the pore size distribution of each catalyst was drawn from the desorption branch of the isotherm using the Barrett-Joyner-Halenda (BJH) method.

X-ray diffraction (XRD) analyses were performed on a Bruker AXS-D8 Advance (Germany) diffractometer using the Co Kα (γ = 1.78 Å) radiation at 35 kV and 40 mA.

H_2 chemisorption at 30 °C was used to measure the Ni dispersion using the ASAP 2010C apparatus from Micrometrics. The catalyst (200 mg) was loaded into a Pyrex tube, and subsequently degassed at room temperature in He for 30 min. After evacuation, the sample was reduced in pure H_2 at 500 °C for 2 h (same as in situ reduction for methanation, see Section 2.3) followed by purging with He for 1 h and adsorption of H_2. Two isotherms were measured in the range of 0.13–60 kPa. The first accounts for reversible physisorption and irreversible chemisorption. The sample was evacuated at 30 °C to desorb reversibly adsorbed H_2. The second isotherm was then measured, accounting only for the reversibly adsorbed H_2. The subtraction of the linear part of the two isotherms gave the total amount of irreversibly chemisorbed H_2. The amount of surface Ni atoms was calculated from the amount of chemisorbed H_2 and the Ni loading, assuming that the chemisorption stoichiometry is H:Ni = 1 and neglecting any contribution of the dopant.

Transmission electron microscopy (TEM) was performed using JEOL-2100 Plus (LaB6) equipped with an Oxford EDX detector.

X-ray photoelectron spectroscopy (XPS) experiments were carried out using an SSX 100/206 spectrometer (Surface Science Instruments, USA) with Al Kα radiation operated at 10 kV and 20 mA. The binding energy scale was calibrated on the Si 2p peak, fixed at 103.5 eV.[22]

H_2-temperature programmed reduction (H_2-TPR) and CO_2 temperature-programmed desorption (CO_2-TPD) measurements were performed on a Hiden Autochem II 2920 instrument with an on-line QIC20 mass spectrometer (MS). For the H_2-TPR, the sample (50 mg) was pretreated in a high purity Ar flow (20 mL/min) at 350 °C for 0.5 h to remove water and other contaminants. Then the sample was cooled down to 30 °C , and a 5% H_2/Ar flow (20 mL/min) was introduced into the system. The MS signal and sample temperature were recorded while the temperature was increased to 900 °C at a heating rate of 10 °C/min. For the CO_2-TPD, 50 mg sample was reduced in-situ at 500 °C for 2 h in a 5% H_2/Ar flow (20 mL/min). After reduction, the sample was purged in an Ar flow (20 mL/min) for 1 h. Then the sample was cooled down to 50 °C, and a 15% CO_2/Ar flow (20 mL/min) was admitted for 1 h. The system was then purged by an Ar flow (20 mL/min) for 1 h at 50 °C. Finally, the catalyst was heated up to 900 °C at a rate of 10 °C /min in the same Ar flow.

In-situ diffuse reflectance infrared Fourier transform spectroscopy (DRIFTS) of CO_2 methanation was carried out on a Nicolet 6700 spectrometer. For each DRIFTS measurement, the catalyst was mixed with KBr (1:5 mass ratio) and 0.03 g of this mix was loaded into the chamber and in-situ reduced at 500 °C for 1 h by a 50% H_2/50% He (20 mL min^{-1}). Then, the gas was changed to He to flush the sample for 30 min at 500 °C to remove residual H_2. Afterwards, the temperature was decreased to 30 °C and then the background was recorded. Subsequently, a CO_2/H_2/He mixture gas (6.7% CO_2/26.8% H_2/66.5% He at a flow 15 mL min^{-1}) was introduced and the temperature was increased in a step mode from 100 to 400 °C with an increment of 50 °C, while the spectra were collected at each temperature when reaching a steady state.

Temperature programmed surface reaction of CO_2 and H_2 (CO_2+H_2 TPSR) and CO and H_2 (CO+H_2 TPSR) experiments were performed on a Hiden Autochem II 2920 instrument with an on-line QIC20 mass spectrometer (MS). 50 mg of catalyst was reduced in-situ at 500 °C for 2 h under a 5% H_2/Ar flow (20 mL/min) and then was purged in an Ar flow (20 mL/min) for 1 h. After cooling down to 50 °C under Ar (20 ml/min), a 20 mL/min flow of 15% CO_2/Ar or 20% CO/Ar was introduced to the reactor for 1 h and purged by Ar gas for 30 min. The TPSR profiles were recorded from 50 °C

to 650 °C with a 5 °C/min heating rate when 5 mL/min of 5% H_2/Ar was flowed into the reactor. The signal of CH_4, CO and CO_2 was examined by MS with the m/z of 15, 28 and 44. For the formaldehyde-temperature programmed surface reaction (HCHO-TPSR) test, 50 mg of reduced catalyst was placed into the reactor and then the reactor was immersed in a HCHO solution (Sigma-Aldrich, 37 wt. % in H_2O, containing 10-15% methanol as stabilizer) for 1 h. After installing the reactor, 20 mL/min of Ar was introduced to the reactor for 30 min. The TPSR profiles were recorded from 30 °C to 250 °C with a 5 °C/min heating rate when 5 mL/min of 5% H_2/Ar was flowed into the reactor. The signal of HCHO and methanol was examined by MS with the m/z of 29 and 31.

2.3. CO_2 methanation.

Catalytic performance was measured in a continuous flow gas-phase microreactor, at atmospheric pressure, as described before.[21] 50 mg of catalyst was placed in the reactor and reduced in situ at 500 °C for 2 h in a 50% H_2/50% He flow (40 mL/min) and then cooled down to 200 °C. Then, a mixture of 10% CO_2 and 40% H_2 balanced with He was introduced to the reactor. The total gas flow rate was 20 mL/min. The catalytic tests were carried out in step mode between 200 °C and 400 °C. Each temperature was maintained for 88 min, allowing for 4 GC analyses. The gas exiting the reactor was analyzed on a gas chromatograph (Varian CP3800), equipped with Hayesep Q, Molsieve 5A, and CP-Sil-5CB columns. The separated gases were analyzed with a flame ionization detector (CH_4) and a thermal conductivity detector (CO and CO_2). All transfer lines were maintained at 125 °C to avoid water condensation. Conversion (X_{CO2}) and selectivity (S_{CH4}) were calculated according to the following equations:

$$X_{CO2} = \frac{F_{CO_2,in} - F_{CO_2,out}}{F_{CO_2,in}}$$

$$S_{CH4} = \frac{F_{CH_4,out}}{F_{CO_2,in} - F_{CO_2,out}}$$

where F is the molar flow rate (after correcting for the volume variations due to the reaction).

3. Results and discussion.

3.1. Catalytic performance.

The CO_2 methanation performance of Ni/SiO_2 and bimetallic $Ni\text{-}M/SiO_2$ catalysts was evaluated in the 200-400 °C temperature range, with a GHSV of 24000 mL g^{-1} h^{-1}. CO_2 conversion and CH_4 selectivity are shown in Fig. 1. In terms of CH_4 selectivity, Ni/SiO_2-r catalyst is over 90% at the reaction temperature at 250 °C and higher. Mn and Co addition have no obvious influence on the CH_4 selectivity, but Cu addition leads to more CO generated over $Ni\text{-}Cu/SiO_2$-r catalyst via the reverse water gas shift (RWGS) reaction ($CO_2 + H_2 \rightarrow CO + H_2O$), resulting in CH_4 selectivity lower than 90% in the whole temperature range. Both Mn and Co addition improved the CO_2 conversion (and methane yield) in the whole temperature range. Notably, Mn addition had a more pronounced effect at low temperature (≤ 250 °C), while Co addition had a more pronounced effect at high temperature (≥ 300 °C). On the contrary, Cu addition consistently has a negative effect on the catalytic activity.

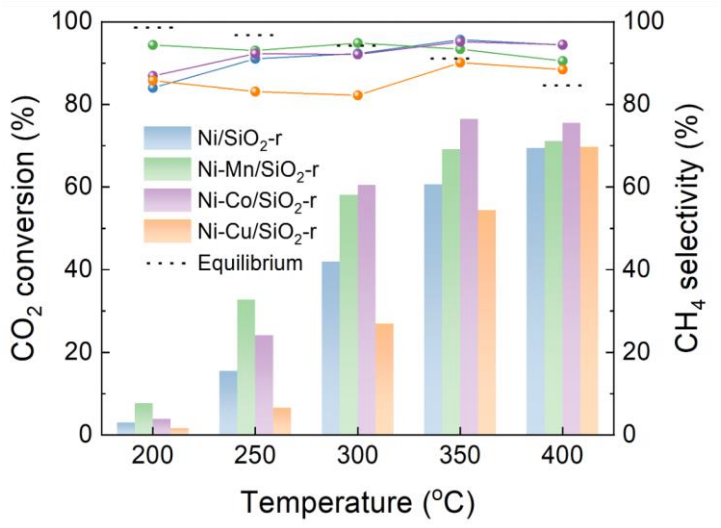

Fig. 1. CO_2 methanation performance in terms of CO_2 conversion and CH_4 selectivity as a function of temperature.

3.2. Catalyst characterization.

The catalyst morphology and nanostructure were explored by TEM, and high-resolution TEM (HRTEM). As shown in Fig. 2a-d, uniformly dispersed particles could

be observed for all reduced catalysts. The average particle size of Ni/SiO_2-r, Ni-Mn/SiO_2-r, Ni-Co/SiO_2-r, and Ni-Cu/SiO_2-r is 3.3, 4.7, 3.8 and 3.5 nm, respectively (listed in Table 1). The clear lattice fringe distances observed on Ni/SiO_2-r is 0.203 nm, corresponding to the Ni (111) plane.[6] On Ni-Mn/SiO_2-r and Ni-Cu/SiO_2-r, the Ni (111) plane could also be confirmed. On the contrary, on Ni-Co/SiO_2-r, the interplanar spacing is 0.216 nm, which is assigned to the NiCo (1-11) plane and indicates the formation of NiCo alloy.[23] Furthermore, Mn_3O_4 (312) plane over Ni-Mn/SiO_2-r, CoO (200) plane over Ni-Co/SiO_2-r and Cu (111) plane over Ni-Cu/SiO_2-r are confirmed by the observation of 0.174 nm, 0.236 nm, and 0.218 nm lattice fringe distances, respectively.[24-26]

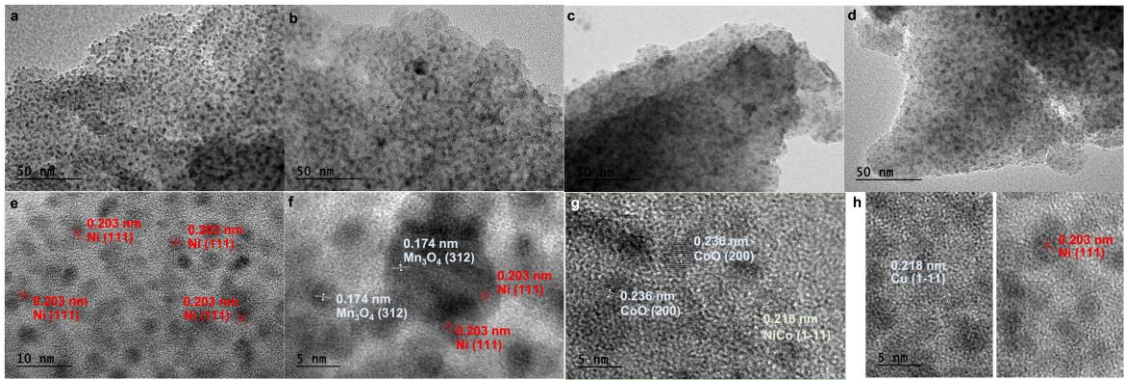

Fig. 2. TEM images of reduced (a, e) Ni/SiO_2-r, (b, f) Ni-Mn/SiO_2-r, (c, g) Ni-Co/SiO_2-r, and (d, h) Ni-Cu/SiO_2-r catalysts.

The catalysts textural properties were measured by N_2 physisorption. As shown in Fig. S1, the catalysts all exhibited type IV adsorption isotherms with a H1-type hysteresis loop, which is characteristic of mesoporous materials[27]. Their average pore diameter is always in the same range of 2.1-2.4 nm (Table 1). Specific surface area and total pore volume are similar for all samples, reaching as high as 510-570 m^2/g and 0.15-0.19 cm^3/g respectively.

Table. 1. Physical Properties of the prepared catalysts.

Sample	S_{BET} (m^2/g)	V_p (cm^3/g)	D_p (nm)	Ni content[a] (%)	Dopant content[a] (%)	Ni particle size[b] (nm)	Dispersion[c] (%)
Ni/SiO_2-r	510	0.15	2.1	18.9	-	3.3	15.8
$Ni-Mn/SiO_2$-r	539	0.19	2.4	18.3	5.1	4.7	12.4
$Ni-Co/SiO_2$-r	564	0.16	2.2	18.2	4.7	3.8	13.4
$Ni-Cu/SiO_2$-r	566	0.14	2.2	18.7	4.6	3.5	14.1

[a] Determined by ICP-AES measurement.

[b] Obtained from the TEM results.

[c] Determined by H_2 chemisorption.

The catalyst crystalline structure was determined by XRD (Fig. 3). All samples exhibited a broad diffraction signal centered at 2θ ~23°, which is ascribed to the amorphous silica matrix.[28] For the calcined samples, two weak and broad diffraction peaks at 37.1° and 43.2° can be assigned to the (111) and (200) planes of NiO.[6] After being reduced under H_2, no obvious diffraction peaks are detected in the reduced samples, suggesting that the expectedly formed Ni particles are small. Consistently, a high Ni dispersion value (15.8%) was determined by H_2 chemisorption measurement for Ni/SiO_2. For metal-doped catalysts, the dispersion remained in the same range, yet slightly lower (listed in Table 1), which points to slightly larger particles.

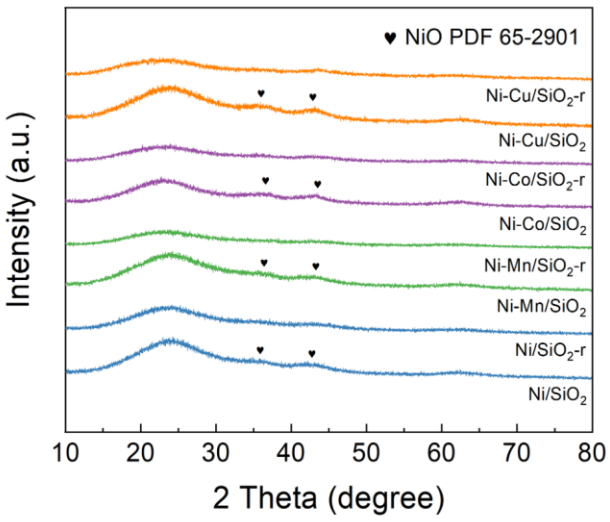

Fig. 3. XRD patterns of the calcined and reduced catalysts.

The reduction behavior of calcined catalysts was investigated using H_2-TPR measurements (Fig. 4a). Two H_2 consumption peaks centered at 373 °C and 565 °C

were fitted for Ni/SiO_2 catalysts, which correspond to the reduction of Ni^{2+} to metallic Ni^0, with the contribution at higher temperature associated to NiO particles in stronger interaction with the SiO_2 matrix. Mn, Co, or Cu addition was found to facilitate the reduction of Ni species as the corresponding reduction peaks shifted to lower temperatures compared to pristine Ni/SiO_2 catalysts. Additional peaks are observed at 740 °C for $Ni\text{-}Co/SiO_2$ and at 257 °C for $Ni\text{-}Cu/SiO_2$, assigned to the reduction of cobalt oxide and copper oxide, respectively.[29-31] A distinct reduction of Mn oxide was not observed (possibly overlapped with the reduction of Ni oxide).

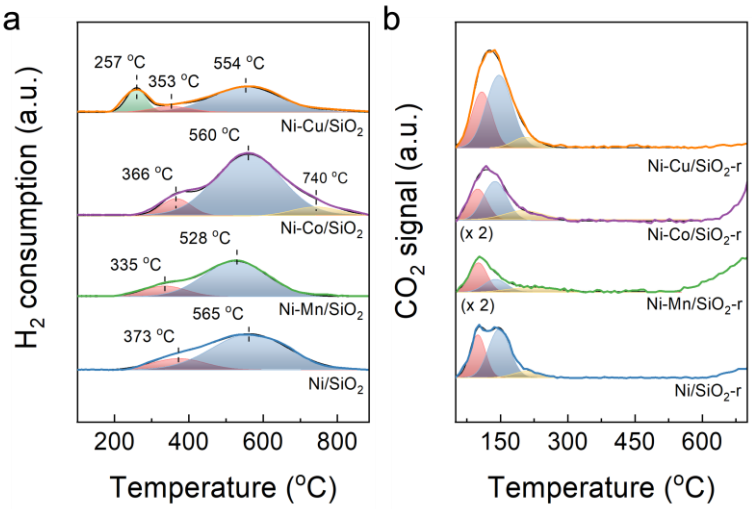

Fig. 4. (a) H_2-TPR profiles of the calcined catalysts; (b) CO_2-TPD profiles of the reduced catalysts.

The chemical state and surface compositions of the reduced catalysts were determined by XPS. As shown in the high-resolution Ni $2p_{3/2}$ spectra (Fig. 5a), the peak at 852.6 eV observed on all reduced catalysts confirms the presence of metallic Ni.[32] Furthermore, the peak at 855.7 eV with a broad satellite at 861.7 eV is associated to the presence of NiO, which can be explained by the re-oxidation of the surface of small Ni nanoparticles surface, in ambient air.[33] The chemical state of the promoters (Mn, Co, and Cu) was also analyzed (Fig. 5b). The spectrum of Mn $2p_{3/2}$ in $Ni\text{-}Mn/SiO_2$-r can be deconvoluted into three peaks with binding energies of 644.7 eV, 641.3 eV, and 639.8 eV attributed to Mn^{4+}, Mn^{3+} and Mn^{2+}, respectively.[34, 35] In the high-resolution spectrum of Co $2p_{3/2}$ of $Ni\text{-}Co/SiO_2$-r, the peak at 782.1 eV accompanied by a broad satellite peak at 786.8 eV are attributed to surface Co^{2+} species, and the weak shoulder

peak at around 776.9 eV can be linked to the presence of Co^0 species.[36] Thus, while showing somewhat more reduced Mn $2p_{3/2}$ and Co $2p_{3/2}$ peaks than in the calcined catalysts (Ni-Mn/SiO_2 and Ni-Co/SiO_2, see Fig. S2), the reduced catalysts still show a majority of oxidized doping agents (Mn^{4+} and Mn^{3+} on the one hand and Co^{2+} on the other hand). This is consistent with the absence of a distinct reduction peak in H_2-TPR. On the contrary, the Cu $2p_{3/2}$ spectrum from Ni-Cu/SiO_2-r shows only one peak attributed to Cu^0 species, at around 933.0 eV.[37] Thus, the partly oxidized Cu found in Ni-Cu/SiO_2 (Fig. S2) is fully converted to metallic Cu upon reduction, which is consistent with the obvious additional reduction peak for the Ni-Cu/SiO_2 catalyst in H_2-TPR.

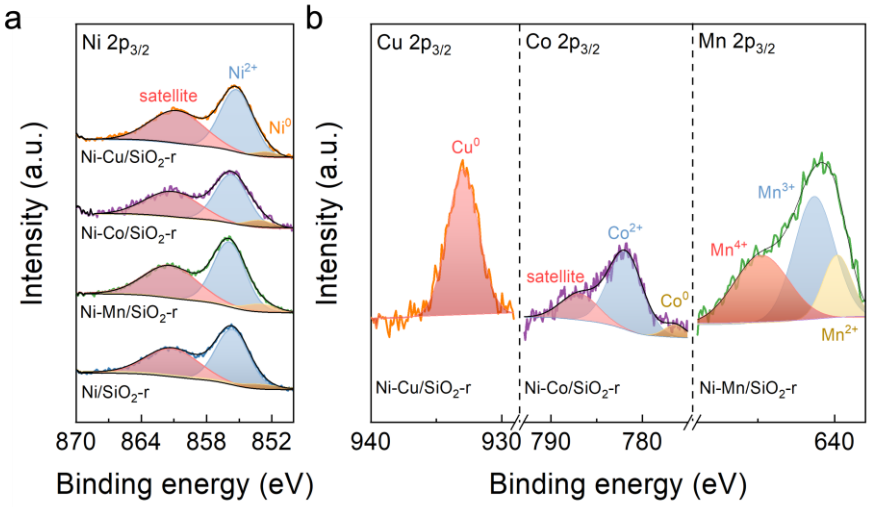

Fig. 5. XPS spectra of (a) Ni $2p_{3/2}$, (b) Mn $2p_{3/2}$, Co $2p_{3/2}$, and Cu $2p_{3/2}$ over the different reduced catalysts.

CO_2-TPD experiments were performed to characterize the surface basicity (Fig. 4b). CO_2 desorption events – characterized by their intensity and temperature – can reveal the amount and strength of different CO_2 adsorption sites. The peak appearing at around 100 °C is attributed to physisorbed CO_2.[38, 39] Furthermore, three distinct desorption events can be observed at higher temperature (ca. 150 °C, ca. 205 °C, and over 550 °C), corresponding to three kinds of adsorbed CO_2 species over the weak, medium and strong basic site, which exist in the form of bicarbonate, monodentate carbonate and bidentate carbonate species.[6] A series of works indicated that the catalytic activity can be promoted by increasing the number of weak and medium basic sites but is not

correlated with the strong basic sites (which are thought to suppress further hydrogenation).[40, 41] The amount of CO_2 adsorption at weak and medium basic sites is listed in Table 2. It can be seen that Ni-Cu/SiO_2-r possesses higher weak and medium basicity than Ni/SiO_2-r, while Ni-Mn/SiO_2-r and Ni-Co/SiO_2-r possess much lower weak and medium basicity than Ni/SiO_2-r.

Table 2. The CO_2-TPD analyses of the reduced catalysts.

	Weak basicity	Medium basicity
Ni/SiO_2-r	3.29	0.55
Ni-Mn/SiO_2-r	0.45	0.35
Ni-Co/SiO_2-r	1.45	0.54
Ni-Cu/SiO_2-r	5.97	0.82

Dispersion, reducibility, and basicity are the key factors usually proposed to govern catalytic performance.[42] Herein, the addition of Cu (compared with pristine Ni/SiO_2) was shown to lead to (i) similar dispersion (H_2 chemisorption) , (ii) increased reducibility (H_2-TPR), and (iii) increased basicity (CO_2-TPD). All three factors should be favorable, and should point to even or higher catalytic performance. Yet, Ni-Cu/SiO_2 exhibited the lowest activity. The addition of Mn and Co resulted in similar dispersion and increased reducibility (compared with pristine Ni/SiO_2) but decreased basicity. These last effects could have been expected to detrimental to catalytic performance. However, a higher catalytic performance was obtained for the Ni-Mn/SiO_2 and Ni-Co/SiO_2. Overall, in this catalyst system, there must be another factor playing a key role on the methanation activity. To understand this apparent discrepancy, we propose to investigate the mechanism of the CO_2 methanation reaction, as it occurs on the various catalysts.

3.3. Investigation of the CO_2 Methanation Mechanism by In Situ DRIFTS and TPSR Experiments.

In general, the possible CO_2 methanation reaction pathways can be divided into three categories: the formate pathway, the RWGS+CO-hydrogenation pathway and the direct C−O bond cleavage pathway.[42] In this study, in-situ DRIFTS and TPSR experiments were carried out in a reacting mixture of CO_2/H_2, in an attempt to identify the surface

species that form during reaction and thereby enhance our understanding of the possible CO_2 methanation pathways over the studied catalysts.

Fig. 6 shows the DRIFT spectra recorded in CO_2 methanation conditions over the four catalysts, from 100 °C to 400 °C. For Ni/SiO_2-r (Fig. 6a), two main species are visible at 100 °C, namely carbonate and carbonyl species. In detail, monodentate carbonate (1512 cm^{-1}), bidentate carbonate (1462 cm^{-1}) and bicarbonate (1388 cm^{-1}) can be observed.[43] The presence of these carbonates as the CO_2-derived surface species is consistent with CO_2-TPD results. As the temperature increases, the bands of those carbonate species become less intense, and the peak attributed to bicarbonate disappears totally at 250 °C. Meanwhile, the vibration modes of monodentate formates (1330 cm^{-1}) and bidentate formates (1369 cm^{-1})[6] appear with high intensity at 150 °C and 250 °C respectively. It has been reported that monodentate formates and bidentate formates can be derived from the hydrogenation of monodentate carbonates and bidentate carbonates.[41] In addition to carbonate and formate species, the bands for 2-fold carbonyl species (1947 cm^{-1}) and 3-fold carbonyl species (1833 cm^{-1})[6] can be clearly seen from 100 °C. These carbonyl species adsorbed on Ni sites are thought to originate from the dissociative adsorption of CO_2.[44] It seems possible that the adsorbed carbonyl species can further react with the adsorbed H atoms on Ni sites to produce formyl (*HCO) species, as indicated by the band at 1747 cm^{-1}[45], and the formyl species can be subsequently hydrogenated towards CH_4. Furthermore, formaldehyde species (1123 cm^{-1}) and methoxy species (1044 cm^{-1}) also appear as intermediate.[45, 46]

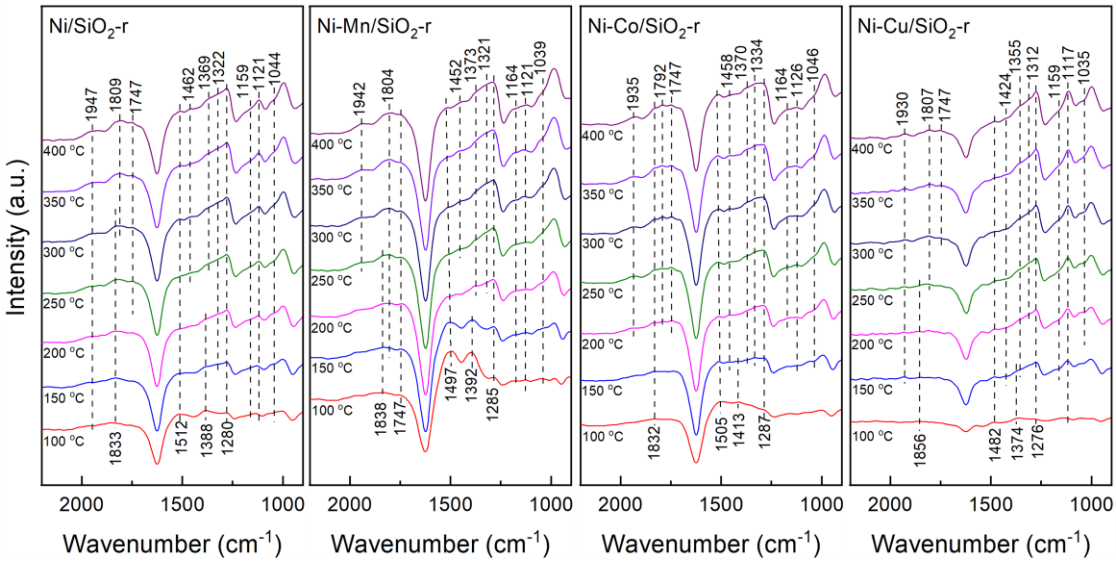

Fig. 6. CO_2 methanation DRIFTS experiments on Ni/SiO_2-r, Ni-Mn/SiO_2-r, Ni-Co/SiO_2-r, and Ni-Cu/SiO_2-r catalysts.

For bimetallic Ni-M/SiO_2-r catalysts (Fig. 6b-6d), carbonate and carbonyl species can be observed with higher intensity (Ni-Mn/SiO_2-r, Ni-Co/SiO_2-r) or lower intensity (Ni-Cu/SiO_2-r) as compared to those over Ni/SiO_2-r. Furthermore, the peak intensity of formate species (ca. 1312 cm^{-1} and 1355 cm^{-1}) and formaldehyde species (ca. 1123 cm^{-1}) shows clear difference for those four catalysts. Specifically, the peak intensity of the formate intermediate increases following the sequence of Ni-Cu/SiO_2-r < Ni/SiO_2-r < Ni-Mn/SiO_2-r < Ni-Co/SiO_2-r (Fig. 7a), while the peak intensity of formaldehyde intermediate increases following the sequence of Ni-Mn/SiO_2-r < Ni-Co/SiO_2-r < Ni/SiO_2-r < Ni-Cu/SiO_2-r (Fig. 7b).

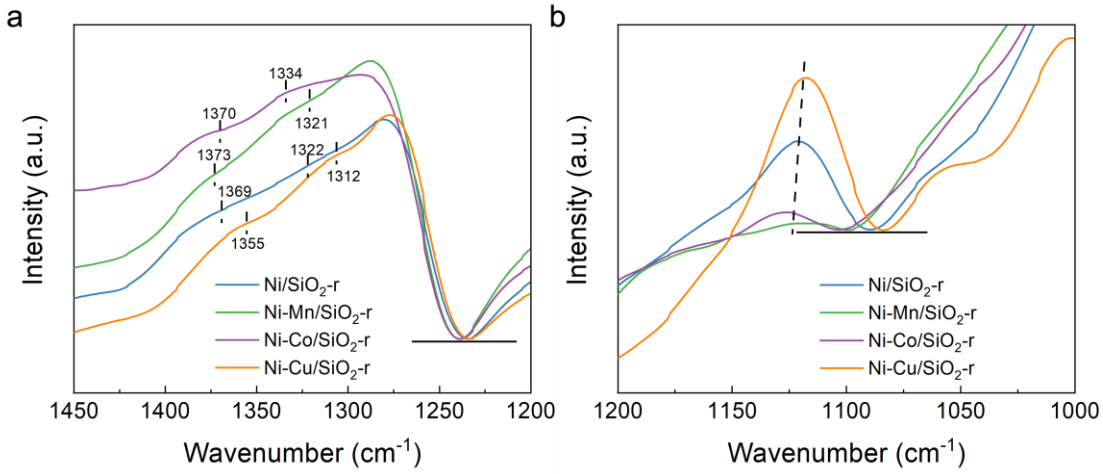

Fig. 7. Comparison of peak intensity of (a) formate intermediate and (b) formaldehyde intermediate.

As shown in our previous work[21], monodentate carbonate species can be hydrogenated to CH_4 via the formate pathway, in which the formate formation is the rate determining step. Carbonyl species derived from the dissociation of CO_2 on the catalyst surface is hydrogenated to CH_4 via the RWGS+CO hydrogenation pathway, in which the rate determining step is the formation of methoxy from formaldehyde.[21] In this context, DRIFTS results suggest that the formation of formate could be facilitated by Mn and Co addition, as indicated by the higher peak intensity of formate over Ni-Co/SiO_2-r and Ni-Mn/SiO_2-r compared with Ni/SiO_2-r (Ni-Co/SiO_2-r > Ni-Mn/SiO_2-r > Ni/SiO_2-r). That is, Mn and Co addition could enhance the formate pathway, and Co addition exhibits a more positive effect on this pathway.

Mn and Co addition appear to facilitate the formation of methoxy from formaldehyde as suggested by the lower peak intensity of formaldehyde over Ni-Mn/SiO_2-r and Ni-Co/SiO_2-r compared with Ni/SiO_2-r (Ni-Mn/SiO_2-r < Ni-Co/SiO_2-r < Ni/SiO_2-r). Correspondingly, Mn and Co addition enhance the RWGS+CO hydrogenation pathway, with the former showing stronger enhancement effect. To confirm the effect of dopants on the transformation of formaldehyde, we performed HCHO-TPSR experiments. In Fig. 8a, the curve of m/z = 29 represents the desorption of formaldehyde, and the curve of m/z = 31 represents the desorption of methanol (methanol is present as stabilizer in the HCHO solution). Each of these curves only have one desorption peak. The curve of m/z = 15, however, shows two distinct desorption peaks. m/z = 15 could represent both methanol and methane. Considering the same trend between the first peak of the m/z = 15 curve and the m/z = 31 curve (methanol), the first peak of the m/z = 15 curve is attributed to the desorption of methanol. Thus, the formation of CH_4 is revealed by the second peak of the m/z = 15 curve. Similar curves are observed for the three bimetallic catalysts (Fig. S3), and the curves of m/z = 15 of the four catalysts are shown in Fig. 8b. The Ni/SiO_2-r, Ni-Mn/SiO_2-r, Ni-Co/SiO_2-r, and Ni-Cu/SiO_2-r catalysts exhibit CH_4 formation breakthroughs at 167 °C, 160 °C, 162 °C, and 181 °C respectively and reach maximum at 206 °C, 197 °C, 201 °C, and 240 °C respectively. The breakthrough and maximum of CH_4 production at lower temperatures demonstrate that Ni-Mn/SiO_2-

r and Ni-Co/SiO_2-r are intrinsically more active than Ni/SiO_2-r for the hydrogenation of formaldehyde to CH_4, and Mn addition show a better effect than Co addition. On the contrary, Cu addition appears to inhibit the hydrogenation of formaldehyde to CH_4.

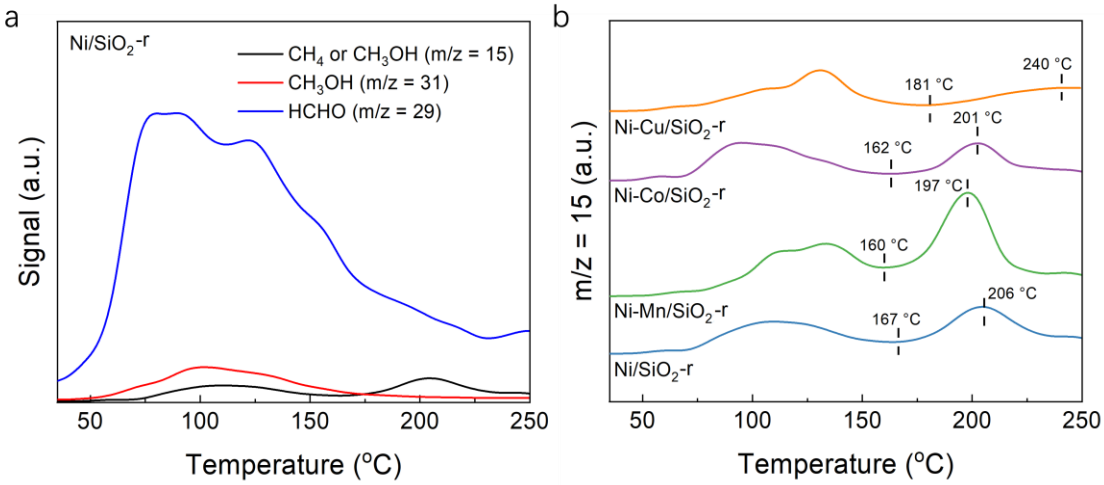

Fig. 8. (a) The curves of m/z = 15, 29, and 31 in HCHO-TPSR over Ni/SiO_2-r. (b) The curve of m/z = 15 in HCHO-TPSR over the reduced catalysts.

The rate determine step of RWGS+CO hydrogenation pathway has a lower energy barrier compared with that of formate pathway.[21] The stronger promotion effect of Mn on the hydrogenation of formaldehyde to CH_4 (the rate determine step of RWGS+CO hydrogenation pathway) is revealed by the highest activity of Ni-Mn/SiO_2-r at low temperature (≤ 250 °C). When the reaction temperature is higher than 300 °C, Ni-Co/SiO_2-r catalyst has the highest activity because Co promotes the formation of formate species (the rate determine step of formate pathway) to the utmost extent. On the contrary, Cu addition inhibits the formation of formate and the transformation of formaldehyde to methoxy, and thus the performance of Ni-Cu/SiO_2-r catalyst decreases compared to Ni/SiO_2-r catalyst.

CO_2+H_2 TPSR tests were also carried out to explore how CO_2 molecules dynamically interact with the catalysts surface during CH_4 production. Specifically, CO_2 was firstly adsorbed and then maintained under a H_2 atmosphere while increasing the temperature. As shown in Fig. 9, the total amount of CH_4 formed over the prepared catalysts decreases in the order of Ni-Cu/SiO_2-r > Ni /SiO_2-r > Ni-Co/SiO_2-r > Ni-Mn/SiO_2-r, which is consistent with the amount of adsorbed CO_2 measured in CO_2-

TPD experiments (i.e. with total basicity). After deconvoluting the profiles, three CH_4 formation peaks can be identified for all the prepared catalysts. Based on a previous mechanistic study[21], we propose to assign peaks α, β, and γ (see Fig. 9) to the CH_4 formed via the RWGS+CO hydrogenation pathway, formate pathway, and C-O cleavage pathway, respectively. For Ni-Mn/SiO_2, the α peak shifts to lower temperature, indicating again that Mn addition facilitates the CH_4 formation via the RWGS+CO hydrogenation pathway. For Ni-Co/SiO_2, the α peak is unaffected but the β peak shifts to lower temperature, suggesting that Co addition facilitates the CH_4 formation via the formate pathway. On the contrary, both the α and the β peaks shift to higher temperatures for Ni-Cu/SiO_2, indicating the Cu addition inhibits the CH_4 formation via the RWGS+CO hydrogenation and formate pathway.

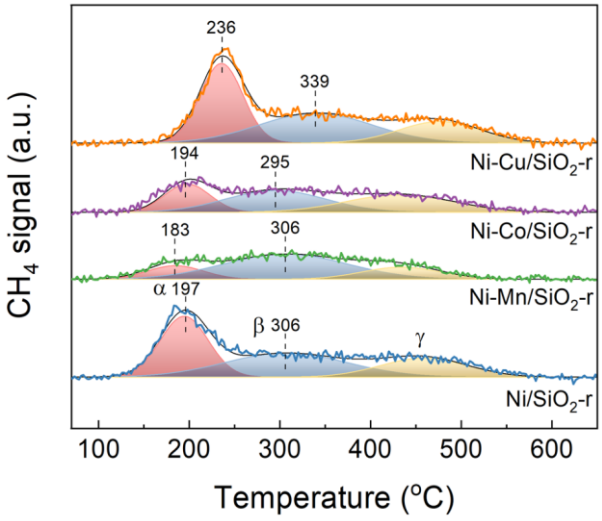

Fig. 9. TPSR over reduced catalysts.

Based on the results of in-situ DRIFTS and TPSR, the promotion effect of Mn and Co addition can be visualized. RWGS+CO hydrogenation pathway is dominant at low temperature. Mn addition facilitates the RWGS+CO hydrogenation pathway to the greatest extent, which leads to the highest activity of Ni-Mn/SiO_2 at lower temperature. The formate pathway can proceed in parallel but is more important at higher temperature. Co addition has the highest promotion effect on the formate pathway, which leads to the highest activity of Ni-Co/SiO_2 at higher temperature.

4. Conclusion

In summary, a series of bimetallic Ni-M/SiO_2 mesoporous catalysts (M = Mn, Co, and Cu) were synthesized by sol-gel method and used for the CO_2 methanation reaction. Ni-Mn/SiO_2 and Ni-Co/SiO_2 shows higher activity, while Ni-Cu/SiO_2 shows lower activity than the pristine, unpromoted, Ni/SiO_2-r catalyst. The effect of doping on dispersion, reducibility and basicity do not seem to explain the activity trends. Instead, doping appears to affect the methanation mechanism, and this is shown to play the most critical role to determining the catalytic performance. Both the RWGS+CO hydrogenation pathway and the formate pathway are identified as active CO_2 methanation mechanisms, with the former being dominant at lower temperature (below 250 °C). Cu addition inhibits those two pathways and results in a lower catalytic activity of Ni-Cu/SiO_2 compared with Ni/SiO_2. RWGS+CO hydrogenation pathway was promoted to the greatest extent by the Mn addition, and formate pathway could be enhanced to the greatest extent by the Co addition. Correspondingly, Ni-Mn/SiO_2 and Ni-Co/SiO_2 shows the highest performance at lower and higher temperature, respectively.

Acknowledgements

YRZ thanks the CSC for his PhD fellowship. DPD thanks the Francqui Foundation for the Francqui Research Professor chair. François Devred is acknowledged for the technical and logistical help.

Reference

[1] N. Mac Dowell, P.S. Fennell, N. Shah, G.C. Maitland, The role of CO2 capture and utilization in mitigating climate change, Nature Climate Change, 7 (2017) 243-249.

[2] S.M. Kim, P.M. Abdala, M. Broda, D. Hosseini, C. Copéret, C. Müller, Integrated CO2 Capture and Conversion as an Efficient Process for Fuels from Greenhouse Gases, ACS Catalysis, 8 (2018) 2815-2823.

[3] R.E. Siegel, S. Pattanayak, L.A. Berben, Reactive Capture of CO2: Opportunities and Challenges, ACS Catalysis, 13 (2023) 766-784.

[4] L. Li, S. Miyazaki, S. Yasumura, K.W. Ting, T. Toyao, Z. Maeno, K.-i. Shimizu, Continuous CO2 Capture and Selective Hydrogenation to CO over Na-Promoted Pt Nanoparticles on Al2O3, ACS Catalysis, 12 (2022) 2639-2650.

[5] J.R. Khusnutdinova, J.A. Garg, D. Milstein, Combining Low-Pressure CO2 Capture and Hydrogenation To Form Methanol, ACS Catalysis, 5 (2015) 2416-2422.

[6] P. Hongmanorom, J. Ashok, P. Chirawatkul, S. Kawi, Interfacial synergistic catalysis over Ni nanoparticles encapsulated in mesoporous ceria for CO2 methanation, Applied Catalysis B: Environmental, 297 (2021) 120454.
[7] K. Mori, T. Taga, H. Yamashita, Isolated Single-Atomic Ru Catalyst Bound on a Layered Double Hydroxide for Hydrogenation of CO2 to Formic Acid, ACS Catalysis, 7 (2017) 3147-3151.
[8] L. Wang, S. He, L. Wang, Y. Lei, X. Meng, F.-S. Xiao, Cobalt–Nickel Catalysts for Selective Hydrogenation of Carbon Dioxide into Ethanol, ACS Catalysis, 9 (2019) 11335-11340.
[9] M.M.F. Hasan, L.M. Rossi, D.P. Debecker, K.C. Leonard, Z. Li, B.C.E. Makhubela, C. Zhao, A. Kleij, Can CO2 and Renewable Carbon Be Primary Resources for Sustainable Fuels and Chemicals?, ACS Sustainable Chemistry & Engineering, 9 (2021) 12427-12430.
[10] N. Rui, X. Zhang, F. Zhang, Z. Liu, X. Cao, Z. Xie, R. Zou, S.D. Senanayake, Y. Yang, J.A. Rodriguez, C.-J. Liu, Highly active Ni/CeO2 catalyst for CO2 methanation: Preparation and characterization, Applied Catalysis B: Environmental, 282 (2021) 119581.
[11] J. Li, A. Slassi, X. Han, D. Cornil, M.-H. Ha-Thi, T. Pino, D.P. Debecker, C. Colbeau-Justin, J. Arbiol, J. Cornil, M.N. Ghazzal, Tuning the Electronic Bandgap of Graphdiyne by H-Substitution to Promote Interfacial Charge Carrier Separation for Enhanced Photocatalytic Hydrogen Production, Advanced Functional Materials, 31 (2021) 2100994.
[12] X. Xu, H.-C. Chen, L. Li, M. Humayun, X. Zhang, H. Sun, D.P. Debecker, W. Zhang, L. Dai, C. Wang, Leveraging Metal Nodes in Metal–Organic Frameworks for Advanced Anodic Hydrazine Oxidation Assisted Seawater Splitting, ACS Nano, 17 (2023) 10906-10917.
[13] D. Xu, Y. Wang, M. Ding, X. Hong, G. Liu, S.C.E. Tsang, Advances in higher alcohol synthesis from CO2 hydrogenation, Chem, 7 (2021) 849-881.
[14] P.H. Ho, G.S. de Luna, S. Angelucci, A. Canciani, W. Jones, D. Decarolis, F. Ospitali, E.R. Aguado, E. Rodríguez-Castellón, G. Fornasari, A. Vaccari, A.M. Beale, P. Benito, Understanding structure-activity relationships in highly active La promoted Ni catalysts for CO2 methanation, Applied Catalysis B: Environmental, 278 (2020) 119256.
[15] W.L. Vrijburg, E. Moioli, W. Chen, M. Zhang, B.J.P. Terlingen, B. Zijlstra, I.A.W. Filot, A. Züttel, E.A. Pidko, E.J.M. Hensen, Efficient Base-Metal NiMn/TiO2 Catalyst for CO2 Methanation, ACS Catalysis, 9 (2019) 7823-7839.
[16] A. Quindimil, U. De-La-Torre, B. Pereda-Ayo, J.A. González-Marcos, J.R. González-Velasco, Ni catalysts with La as promoter supported over Y- and BETA- zeolites for CO2 methanation, Applied Catalysis B: Environmental, 238 (2018) 393-403.
[17] G. Garbarino, C. Wang, T. Cavattoni, E. Finocchio, P. Riani, M. Flytzani-Stephanopoulos, G. Busca, A study of Ni/La-Al2O3 catalysts: A competitive system for CO2 methanation, Applied Catalysis B: Environmental, 248 (2019) 286-297.
[18] X. Xu, L. Liu, Y. Tong, X. Fang, J. Xu, D.-e. Jiang, X. Wang, Facile Cr3+-Doping Strategy Dramatically Promoting Ru/CeO2 for Low-Temperature CO2 Methanation: Unraveling the Roles of Surface Oxygen Vacancies and Hydroxyl Groups, ACS Catalysis, 11 (2021) 5762-5775.
[19] Y. Wu, J. Lin, Y. Xu, G. Ma, J. Wang, M. Ding, Transition Metals Modified Ni−M (M=Fe, Co, Cr and Mn) Catalysts Supported on Al2O3−ZrO2 for Low-Temperature CO2 Methanation, ChemCatChem, 12 (2020) 3553-3559.
[20] L. Xu, Y. Cui, M. Chen, X. Wen, C. Lv, X. Wu, C.-e. Wu, Z. Miao, X. Hu, Screening Transition Metals (Mn, Fe, Co, and Cu) Promoted Ni-Based CO2 Methanation Bimetal Catalysts with Advanced Low-Temperature Activities, Industrial & Engineering Chemistry Research, 60 (2021) 8056-8072.

[21] Y. Zhao, V. Girelli, O. Ersen, D.P. Debecker, CO2 methanation with high-loading mesoporous Ni/SiO2 catalysts: Toward high specific activity and new mechanistic insights, Journal of Catalysis, 426 (2023) 283-293.
[22] M. Jacquemin, M.J. Genet, E.M. Gaigneaux, D.P. Debecker, Calibration of the X-Ray Photoelectron Spectroscopy Binding Energy Scale for the Characterization of Heterogeneous Catalysts: Is Everything Really under Control?, ChemPhysChem, 14 (2013) 3618-3626.
[23] S. Ding, L. He, L. Fang, Y. Zhu, T. Li, Z. Lyu, D. Du, Y. Lin, J.-C. Li, Carbon-Nanotube-Bridging Strategy for Integrating Single Fe Atoms and NiCo Nanoparticles in a Bifunctional Oxygen Electrocatalyst toward High-Efficiency and Long-Life Rechargeable Zinc–Air Batteries, Advanced Energy Materials, 12 (2022) 2202984.
[24] H. Chen, Y. Xia, R. Fang, H. Huang, Y. Gan, C. Liang, J. Zhang, W. Zhang, X. Liu, Effects of Nd-modification on the activity and SO2 resistance of MnOx/TiO2 catalysts for low-temperature NH3-SCR, New Journal of Chemistry, 42 (2018) 12845-12852.
[25] X. Peng, J. Zhang, T. Cen, Z. Ye, Y. Liu, D. Yuan, Co(OH)2-NiCo2O4 hybrid nanosheets coupled with N-doping reduced graphene oxide as efficient electrocatalysts for Zn-air batteries, Journal of Alloys and Compounds, 872 (2021) 159441.
[26] M. Sun, W. Zhang, Z. Liu, G. Wang, Direct observations on the crystal structure evolution of nano Cu-precipitates in an extremely low carbon steel, Materials Letters, 187 (2017) 49-52.
[27] K. Li, X. Chang, C. Pei, X. Li, S. Chen, X. Zhang, S. Assabumrungrat, Z.-J. Zhao, L. Zeng, J. Gong, Ordered mesoporous Ni/La2O3 catalysts with interfacial synergism towards CO2 activation in dry reforming of methane, Applied Catalysis B: Environmental, 259 (2019) 118092.
[28] B. Zhao, P. Liu, S. Li, H. Shi, X. Jia, Q. Wang, F. Yang, Z. Song, C. Guo, J. Hu, Z. Chen, X. Yan, X. Ma, Bimetallic Ni-Co nanoparticles on SiO2 as robust catalyst for CO methanation: Effect of homogeneity of Ni-Co alloy, Applied Catalysis B: Environmental, 278 (2020) 119307.
[29] P. Shafiee, S.M. Alavi, M. Rezaei, Solid-state synthesis method for the preparation of cobalt doped Ni–Al2O3 mesoporous catalysts for CO2 methanation, International Journal of Hydrogen Energy, 46 (2021) 3933-3944.
[30] Q. Liu, B. Bian, J. Fan, J. Yang, Cobalt doped Ni based ordered mesoporous catalysts for CO2 methanation with enhanced catalytic performance, International Journal of Hydrogen Energy, 43 (2018) 4893-4901.
[31] N. Gutta, V.K. Velisoju, A. Chatla, V. Boosa, J. Tardio, J. Patel, V. Akula, Promotional Effect of Cu and Influence of Surface Ni–Cu Alloy for Enhanced H2 Yields from CH4 Decomposition over Cu-Modified Ni Supported on MCM-41 Catalyst, Energy & Fuels, 32 (2018) 4008-4015.
[32] Z. Hao, J. Shen, S. Lin, X. Han, X. Chang, J. Liu, M. Li, X. Ma, Decoupling the effect of Ni particle size and surface oxygen deficiencies in CO2 methanation over ceria supported Ni, Applied Catalysis B: Environmental, 286 (2021) 119922.
[33] Y. Xie, J. Chen, X. Wu, J. Wen, R. Zhao, Z. Li, G. Tian, Q. Zhang, P. Ning, J. Hao, Frustrated Lewis Pairs Boosting Low-Temperature CO2 Methanation Performance over Ni/CeO2 Nanocatalysts, ACS Catalysis, 12 (2022) 10587-10602.
[34] H. Li, G. Lu, Q. Dai, Y. Wang, Y. Guo, Y. Guo, Efficient low-temperature catalytic combustion of trichloroethylene over flower-like mesoporous Mn-doped CeO2 microspheres, Applied Catalysis B: Environmental, 102 (2011) 475-483.

[35] Y. Yang, J. Huang, S. Wang, S. Deng, B. Wang, G. Yu, Catalytic removal of gaseous unintentional POPs on manganese oxide octahedral molecular sieves, Applied Catalysis B: Environmental, 142-143 (2013) 568-578.
[36] A.H. Braga, D.C. de Oliveira, A.R. Taschin, J.B.O. Santos, J.M.R. Gallo, J.M. C. Bueno, Steam Reforming of Ethanol Using Ni–Co Catalysts Supported on MgAl2O4: Structural Study and Catalytic Properties at Different Temperatures, ACS Catalysis, 11 (2021) 2047-2061.
[37] L.-C. Chen, S.D. Lin, The ethanol steam reforming over Cu-Ni/SiO2 catalysts: Effect of Cu/Ni ratio, Applied Catalysis B: Environmental, 106 (2011) 639-649.
[38] L. Roldán, Y. Marco, E. García-Bordejé, Origin of the Excellent Performance of Ru on Nitrogen-Doped Carbon Nanofibers for CO2 Hydrogenation to CH4, ChemSusChem, 10 (2017) 1139-1144.
[39] G. Varvoutis, M. Lykaki, E. Papista, S.A.C. Carabineiro, A.C. Psarras, G.E. Marnellos, M. Konsolakis, Effect of alkali (Cs) doping on the surface chemistry and CO2 hydrogenation performance of CuO/CeO2 catalysts, Journal of CO2 Utilization, 44 (2021) 101408.
[40] H. Muroyama, Y. Tsuda, T. Asakoshi, H. Masitah, T. Okanishi, T. Matsui, K. Eguchi, Carbon dioxide methanation over Ni catalysts supported on various metal oxides, Journal of Catalysis, 343 (2016) 178-184.
[41] Q. Pan, J. Peng, T. Sun, S. Wang, S. Wang, Insight into the reaction route of CO2 methanation: Promotion effect of medium basic sites, Catalysis Communications, 45 (2014) 74-78.
[42] L. Shen, J. Xu, M. Zhu, Y.-F. Han, Essential Role of the Support for Nickel-Based CO2 Methanation Catalysts, ACS Catalysis, 10 (2020) 14581-14591.
[43] X. Xu, Y. Tong, J. Huang, J. Zhu, X. Fang, J. Xu, X. Wang, Insights into CO2 methanation mechanism on cubic ZrO2 supported Ni catalyst via a combination of experiments and DFT calculations, Fuel, 283 (2021) 118867.
[44] C. Cerdá-Moreno, A. Chica, S. Keller, C. Rautenberg, U. Bentrup, Ni-sepiolite and Ni-todorokite as efficient CO2 methanation catalysts: Mechanistic insight by operando DRIFTS, Applied Catalysis B: Environmental, 264 (2020) 118546.
[45] R.-P. Ye, Q. Li, W. Gong, T. Wang, J.J. Razink, L. Lin, Y.-Y. Qin, Z. Zhou, H. Adidharma, J. Tang, A.G. Russell, M. Fan, Y.-G. Yao, High-performance of nanostructured Ni/CeO2 catalyst on CO2 methanation, Applied Catalysis B: Environmental, 268 (2020) 118474.
[46] S. Zhang, S. Sun, B. Huang, N. Wang, X. Li, UV-Enhanced Formaldehyde Sensor Using Hollow In2O3@TiO2 Double-Layer Nanospheres at Room Temperature, ACS Applied Materials & Interfaces, 15 (2023) 4329-4342.